Inorganic Chemistry

Article

pubs.acs.org/IC

Large Mid-IR Second-Order Nonlinear-Optical Effects Designed by the Supramolecular Assembly of Different Bond Types without IR Absorption

Xiao-Ming Jiang, Guan-E Wang, Zhi-Fa Liu, Ming-Jian Zhang, and Guo-Cong Guo*

State Key Laboratory of Structural Chemistry, Fujian Institute of Research on the Structure of Matter, Chinese Academy of Sciences, Fuzhou, Fujian 350002, People's Republic of China

Supporting Information

ABSTRACT: Two new different-bond-type hybrid compounds, $(Hg_6P_4Cl_3)(PbCl_3)$ (**1**) and $(Hg_{23}P_{12})(ZnCl_4)_6$ (**2**), with supramolecular interactions between host and guest moieties, which based on metal−pnicogen, pnicogen−pnicogen, and metal−halogen bonds were obtained by solid-state reactions. Compounds **1** and **2** show large second-harmonic-generation (SHG) activity and are transparent in the wide mid-IR region, providing an effective route for searching new IR nonlinear-optical material systems by combining two or more different bond types with no IR absorption within a single compound through supramolecular assembly. Theory predications based on first-principles calculations are also performed on the SHG properties of **1** and **2**.

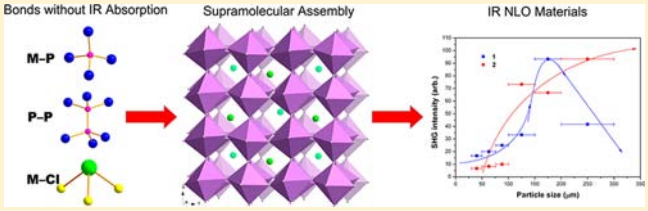

1. INTRODUCTION

Second-order nonlinear-optical (NLO) materials are of current interest and great importance because of their uses in optical signal processing and as new laser sources.[1] Many well-known second-order NLO materials,[2] such as KH_2PO_4 (KDP), $KTiOPO_4$ (KTP), β-BaB_2O_4 (BBO), LiB_3O_5 (LBO), and so on, are based on oxides and are widely used in visible and ultraviolet regions but cannot be used in mid- and far-IR regions because of strong absorption. Up to now, worldwide concerned IR NLO material systems[3] mainly include classical binary and ternary metal pnictides and chalcogenides (GaSe,[4a] $ZnGeP_2$,[4b] $AgGaS_2$,[4c] etc.), quaternary metal chalcogenides ($Li_2Ga_2GeS_6$,[5a] α- and β-$A_2Hg_3M_2S_8$ (A = K, Rb; M = Ge, Sn),[5b] etc.), and binary and ternary metal halides [$HgBr_2$,[6a] $BaMF_4$ (M = Mg, Mn, Co, Ni, Zn),[6b] etc.]. In contrast, different-bond-type hybrid IR NLO materials [$A_2P_2Se_6$ (A = K, Rb),[7a] $A_3Ta_2AsS_{11}$ (A = K, Rb),[7b] etc.] in which at least two obvious different types of bonds exist, such as metal−chalcogen and chalcogen−chalcogen bonds in metal thiotelluites, metal−chalcogen and pnicogen−chalcogen bonds in metal chalcopnictates, and so on, are relatively rare. Many different bond types without IR absorption can be diversely combined to form new materials with noncentrosymmetric structure and no absorption in the IR region, which is indispensable for IR NLO properties. In addition, different-bond-type hybrids may overcome some disadvantages possessed by metal pnictides, chalcogenides, and halides with only one type of bond, such as the low laser damage threshold of $ZnGeP_2$ and $AgGaS_2$ and the poor thermal and chemical stabilities of some metal halides, through complementary and synergistic effects.[8] Therefore, the search in different-bond-type hybrids may be an effective route for discovering new materials with excellent IR NLO properties.

Supramolecular assembly, which can combine a polycation and a polyanion containing different bond types in the same product in a diverse spatial arrangement,[9] is very likely to form different-bond-type hybrids with noncentrosymmetric structure, especially involving functional components containing cations susceptible to second-order Jahn−Teller distortion, such as Pb^{2+}, Sb^{3+}, Se^{4+}, etc., with stereochemically active electron pairs.[10] Guided by these ideas, our exploration on different-bond-type hybrids led to the discovery of two new inorganic supramolecular compounds, $(Hg_6P_4Cl_3)(PbCl_3)$ (**1**) and $(Hg_{23}P_{12})(ZnCl_4)_6$ (**2**), with Hg−P or P−P bonds in the hosts and Pb−Cl or Zn−Cl bonds in the guests. They both show large second-harmonic-generation (SHG) efficiencies of about 2.5 and 1.1 times that of $AgGaS_2$, respectively, and are transparent in the wide IR range (2.5−25 μm). Herein we report their syntheses, crystal structures, and IR NLO properties. Theory predications based on first-principles calculations are also performed on their SHG properties.

2. EXPERIMENTAL SECTION

Reagents and Syntheses. All of the starting materials were used as received without further purification. Single crystals of the two compounds were obtained by solid-state reactions. Compound **1** was crystallized from the reaction containing Hg_2Cl_2 (1.0 mmol, 99.5%), $Hg(CN)_2$ (1.0 mmol, 99.5%), $PbCl_2$ (0.5 mmol, 99.5%), and red phosphorus (2.0 mmol, 99.99%). Compound **2** was crystallized from the reaction containing $HgCl_2$ (0.1 mmol, 99.5%), Hg_2Cl_2 (1.1 mmol,

Received: April 28, 2013
Published: July 9, 2013

   dx.doi.org/10.1021/ic401056t | Inorg. Chem. 2013, 52, 8865−8871

99.5%), zinc (0.6 mmol, 99.99%), and red phosphorus (1.2 mmol, 99.99%). The starting materials were ground into fine powders in a agate mortar and pressed into a pellet, followed by loading into Pyrex tubes, evacuation to 1×10^{-4} Torr, and flame-sealing, and then the tubes were placed into a computer-controlled furnace. The tubes were heated from room temperature to 200 °C at a rate of 50 °C h^{-1} and kept at 200 °C for 2 days, and then they were heated to 340 and 400 °C for **1** and **2**, respectively, at 20 °C h^{-1}, kept at those temperatures for 5 days, and then slowly cooled to 50 °C at a rate of 2.5 °C h^{-1}. Yellow crystals of the title compounds were obtained, and the product yields were about 90% and 80% for **1** and **2**, respectively. An impurity of minor mercury drops was found in the products of both reactions and was easily cleaned up mechanically. Pure crystals of **1** and **2** for physical property measurements were handpicked under a microscope, and their purities were confirmed by a powder X-ray diffraction (XRD) study (Figure 2a). ***Caution!*** *$HgCl_2$, Hg_2Cl_2, $Hg(CN)_2$, and $PbCl_2$ are toxic. Extreme care must be exercised, and some toxic gases may be released when the Pyrex tubes are opened. $HgCl_2$ is water-sensitive, so it is much better if the weighing of reagents, grinding of the mixture, and pressing into pellets are performed in drybox.* Both compounds are stable in the presence of air and water.

Crystal Structure Determination. The respective single crystals of **1** and **2** with suitable dimensions were mounted on glass fiber for single-crystal XRD analysis. The measurements were performed on a Rigaku Saturn 70 CCD diffractometer equipped with graphite-monochromated Mo Kα radiation (λ = 0.71073 Å) at 293 K. The intensity data sets were collected with a ω-scan technique and reduced using *CrystalClear* software.[11] The structures of the two compounds were solved by direct methods and refined by full-matrix least-squares techniques on F^2. All of the calculations were performed with the Siemens *SHELXL*, version 5, package of crystallographic software.[12] The formulas are based on taking collectively into account crystallographically refined compositions and requirements of charge neutrality. Relevant crystallographic data and details of the experimental conditions for **1** and **2** are summarized in Table 1. Atomic coordinates and select interatomic distances are reported in Tables S1–S4 in the Supporting Information (SI).

Powder XRD, Thermogravimertric Analysis (TGA), and Energy-Dispersive X-ray (EDS), IR, and UV–vis–Near-IR (NIR) Diffuse-Reflectance Spectroscopies. The powder XRD patterns (Figure 2a) were collected with a Rigaku DMAX 2500 diffractometer at 40 kV and 100 mA for Cu Kα radiation (λ =1.5406 Å) with a scan speed of 5° min^{-1} at room temperature. The simulated patterns were produced using the *Mercury* program and single-crystal reflection data. TGA studies of **1** and **2** were carried out with a NETZSCH STA 449C instrument under a nitrogen atmosphere. The samples and reference were held in Al_2O_3 crucibles, heated at a rate of 10 °C min^{-1} from room temperature to 800 °C. Semiquantitative microscopic analysis using EDS was performed on a JSM6700F scanning electron microscope on a single crystal, which confirmed the presence of Hg, Pb, P, and Cl in the approximate molar ratio 5.9:1.0:4.3:6.5 and Hg, Zn, P, and Cl in the approximate molar ratio 22.5:6.0:12.6:24.5 for **1** and **2**, respectively. No other elements were detected. The diffuse-reflectance spectra were recorded at room temperature on a computer-controlled Lambda 900 UV–vis–NIR spectrometer equipped with an integrating sphere in the wavelength range of 300–2000 nm. A $BaSO_4$ plate was used as the reference, on which the finely ground powders of the samples were coated. The absorption spectra were calculated from reflection spectra using the Kubelka–Munk function.[13] The IR spectra were recorded using a Nicolet Magna 750 Fourier transform infrared (FT-IR) spectrophotometer in the range of 4000–400 cm^{-1}. Powdery samples were pressed into pellets with KBr. No FT-IR absorption peaks of **1** and **2** are in the range 4000–400 cm^{-1}.

SHG Measurements. Powder SHG measurements on hand-selected crystalline samples were performed on a modified Kurtz–NLO system using 2.05 μm laser radiation. The output signals were detected by a photomultiplier, and a $AgGaS_2$ powder sieved with 150 meshes (~100 μm) was used as a comparison. Compounds **1** and **2** were ground and sieved into several distinct particle size ranges (0–50, 50–76, 76–100, 100–150, 150–200, and 200–300 μm). All of the samples were pressed between glass microscope cover slides and secured with tape in 1-mm-thick aluminum holders containing an 8-mm-diameter hole.

Table 1. Crystal Data and Structure Refinement Parameters for 1 and 2

chemical formula	$(Hg_6P_4Cl_3)(PbCl_3)$ (**1**)	$(Hg_{23}P_{12})(ZnCl_4)_6$ (**2**)
fw	1747.31	6228.23
cryst size (mm^3)	0.10 × 0.10 × 0.10	0.20 × 0.20 × 0.10
cryst syst	cubic	hexagonal
space group	$P2_13$	$P\bar{6}2m$
a (Å)	11.8837(2)	12.9774(7)
c (Å)	11.8837(2)	11.7490(11)
V (Å^3)	1678.24(5)	1713.6(2)
Z	4	1
D_{calcd} (g cm^{-1})	6.916	6.035
μ (mm^{-1})	65.976	54.561
F(000)	2896	2608
θ range (deg)	2.42–25.94	3.14–27.41
index range	$-14 \le h \le 14$, $-14 \le k \le 14$, $-14 \le l \le 12$	$-16 \le h \le 16$, $-16 \le k \le 16$, $-15 \le l \le 15$
measd reflns	14733	14700
indep reflns/R_{int}	1111/0.0713	1470/0.0815
obsd reflns	1110	1039
R1[a] [$I > 2\sigma(I)$]	0.0286	0.0473
wR2[b] (all data)	0.08	0.1193
GOF on F^2	1.087	0.999
Flack parameter	0.00(9)	0.0(3)
$\Delta\rho_{max}/\Delta\rho_{min}$ (e Å^{-3})	2.342/−1.487	3.707/−2.402

[a] $R1 = ||F_o| - |F_c||/|F_o|$. [b] $wR2 = [w(F_o^2 - F_c^2)^2]/[w(F_o^2)^2]^{1/2}$.

Computational Descriptions. The crystallographic data of **1** and **2** determined by single-crystal XRD were used to calculate their electronic band structures, densities of states (DOSs), and optical properties, and no further geometry optimization was performed in the theoretical studies. The calculation was performed with the *CASTEP* code[14] based on density functional theory using a plane-wave expansion of the wave functions. The total energy was calculated within the framework of a nonlocal gradient-corrected approximation, the Perdew–Burke–Ernzerhof (PBE) functional.[15] The interactions between the ionic cores and electrons are described by the norm-conserving pseudopotential,[16] in which the orbital electrons of P $3s^23p^3$, Cl $3s^23p^5$, Hg $5d^{10}6s^2$, Pb $5d^{10}6s^26p^2$, and Zn $3d^{10}4s^2$ are treated as valence electrons. The number of plane waves included in the basis set was determined by a cutoff energy of 750 eV, and the numerical integration of the Brillouin zone was performed using a 4 × 4 × 4 Monkhorst Pack k-point sampling for both **1** and **2**. The convergent criterion of the total energy was set by the default value of the *CASTEP* code.

Calculations of the optical properties described in terms of the complex dielectric function $\varepsilon(\omega) = \varepsilon_1(\omega) + i\varepsilon_2(\omega)$ were made. The imaginary part of the dielectric function $\varepsilon_2(\omega)$ is given in the following equation:[17]

$$\varepsilon_2(\omega) = \frac{2e^2\pi}{\Omega\varepsilon_0} \sum_{k,v,c} |\langle \Psi_k^c | \hat{u}\cdot r | \Psi_k^v \rangle|^2 \delta(E_k^c - E_k^v - E) \quad (1)$$

where $\delta(E_k^c - E_k^v - E)$ denotes the energy difference between the conduction and valence bands at the k point with absorption of energy E, $\hat{u}$ is the vector defining the polarization of the incident electric field, Ω is the volume of the primitive cell, e is the electric charge, Ψ_k^c and Ψ_k^v are the conduction and valence band wave functions at k, respectively, and $\varepsilon_1(\omega)$ can be obtained using the dispersion relationship of Kramers–Kronig:

dx.doi.org/10.1021/ic401056t | Inorg. Chem. 2013, 52, 8865–8871

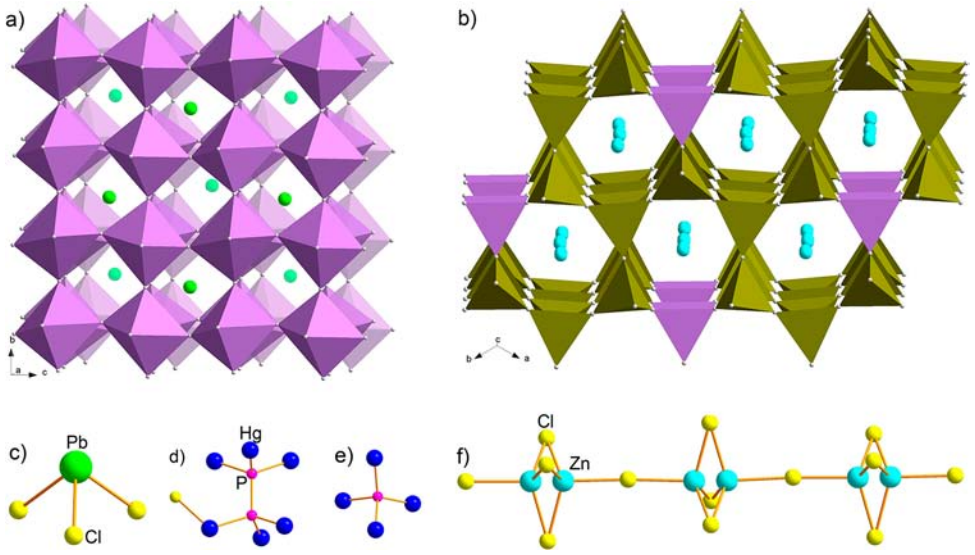

Figure 1. (a) Perovskite-like 3D cationic network of **1** [purple octahedra represent $(Hg_6P_4Cl_3)^+$ units (d)] with discrete triangular pyramidal $(PbCl_3)^-$ anions (c) (represented by Pb atoms only in part a) embedded in half-cavities of it. All Cl atoms in part a are not shown for clarity. (b) 3D cationic network of **2** [purple triangular prisms represent Hg_6P_2 units with a configuration similar to that of part d without the Cl atom; dark-yellow tetrahedra represent Hg_4P units (e)] with $_\infty^1(ZnCl_4)^{2-}$ chiral chain [part f; only Zn atoms are shown in part b for clarity] embedded in the tunnels of it. Two Zn positions in part f are adjacent because of splitting.

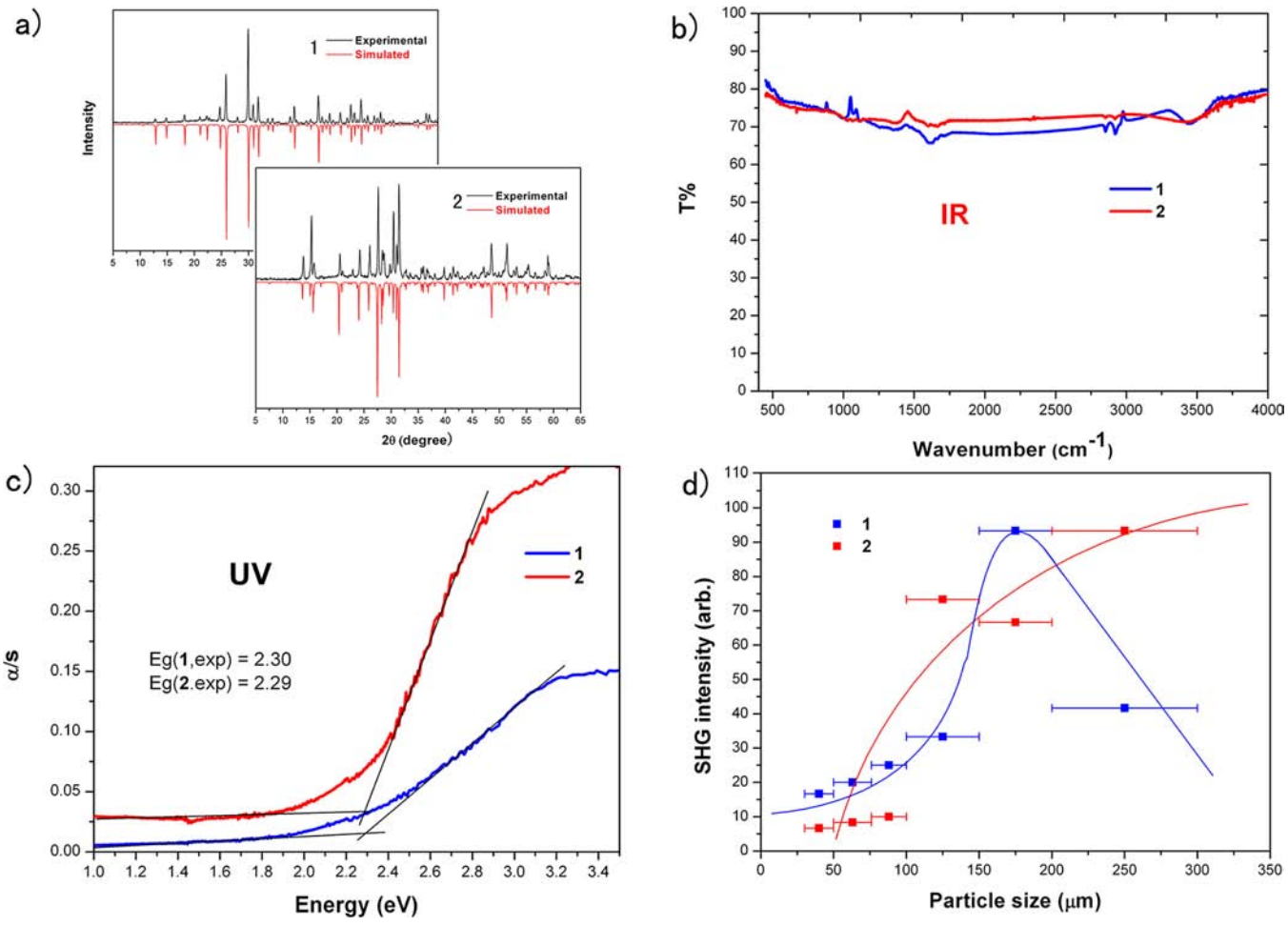

Figure 2. (a) Simulated and experimental powder XRD patterns of **1** and **2** and (b) FT-IR spectra of **1** and **2**. The minor peaks at ~920, ~1640, and ~3300 cm^{-1} can be attributed to water. (c) Absorption spectra of **1** and **2**, converted from UV diffuse-reflectance spectra of **1** and **2**, respectively. (d) SHG signals of **1** and **2** as a function of the particle size. The curve is a guide to the eye and is not a fit to the data.

dx.doi.org/10.1021/ic401056t | Inorg. Chem. 2013, 52, 8865−8871

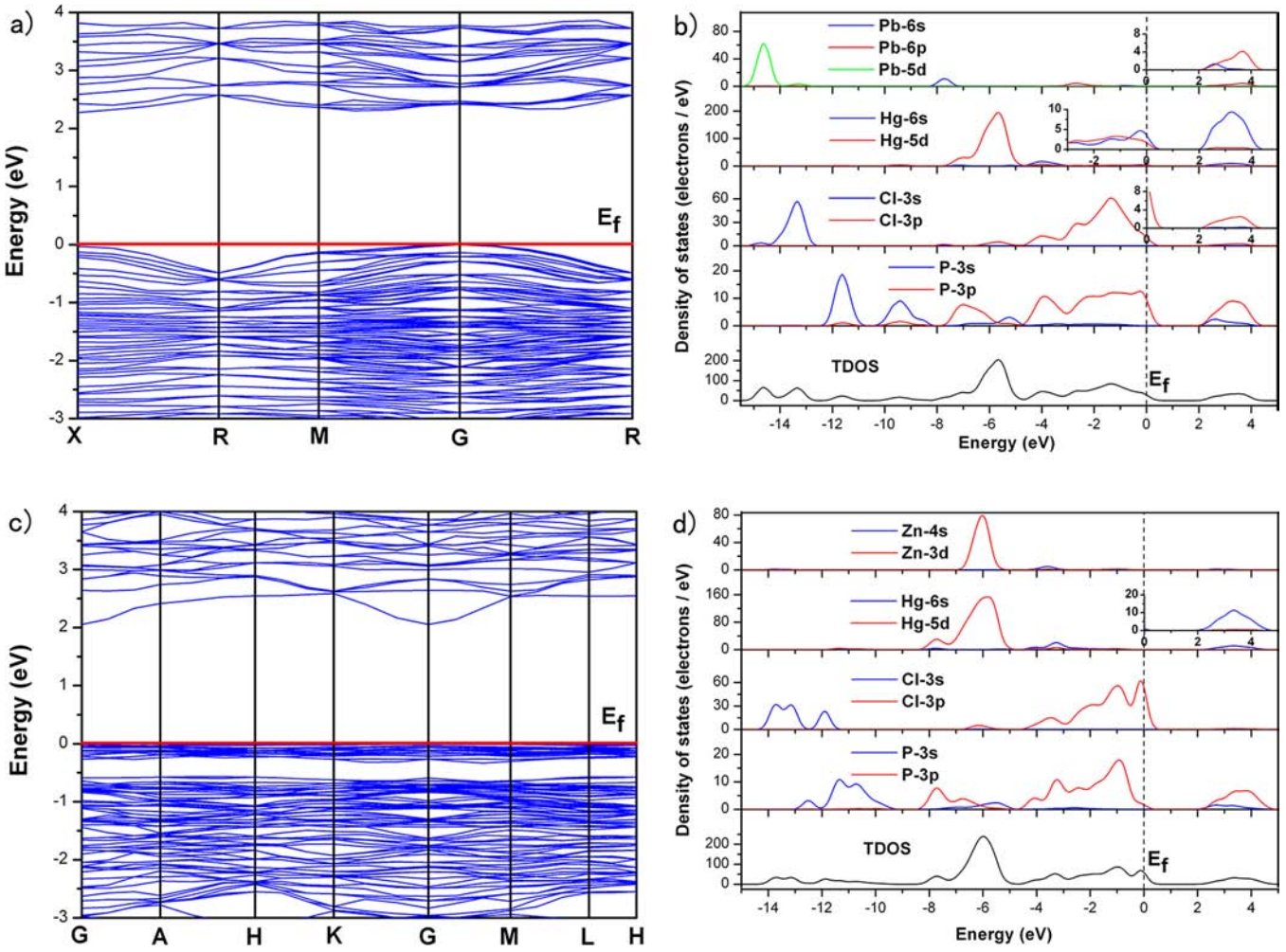

Figure 3. Band structures of **1** (a) and **2** (c) (bands are shown only between −3.0 and 4.0 eV for clarity). Total and partial DOSs of **1** (b) and **2** (d). The energies of less than −15.5 eV for **1** and −15.0 eV for **2** are omitted for clarity. The Fermi level is set at 0 eV for all of the band structures and DOS. The calculated band gaps of **1** and **2** are 2.27 and 2.05 eV, respectively.

$$\varepsilon_1(\omega) = 1 + \frac{2}{\pi} P \int_0^\infty \frac{\omega' \varepsilon_2(\omega')}{\omega'^2 - \omega^2} \, d\omega' \tag{2}$$

where P in front of the integral means the principal value. The first-order nonresonant susceptibility at the low-frequency region is given by $\chi^{(1)}_{ii}(\omega) = \varepsilon_{ii}(\omega) - 1$, and the second-order susceptibilities can be expressed in terms of the first-order susceptibilities as follows:[18]

$$\chi^{(2)}_{ijk}(\omega_3, \omega_1, \omega_2) = \frac{ma}{N^2 e^3} \chi^{(1)}_{ii}(\omega_3) \chi^{(1)}_{jj}(\omega_1) \chi^{(1)}_{kk}(\omega_2) \tag{3}$$

which are derived from a classical anharmonic oscillator model. m, e, and N are the electron mass, electron charge, and number density of the atoms, respectively, and the parameter a characterizing the nonlinearity of the response can be obtained from experimental or theoretical estimations.

3. RESULTS AND DISCUSSION

The 3D cationic framework (Figure 1) of **1** is built of the P, Hg, and one of two nonequivalent Cl atoms. Two independent P atoms each possess tetrahedral coordination of one P atom and three Hg atoms and are joined into pairs by a P−P bond (Figure 1d). Each pair is surrounded by six Hg atoms (Hg1 and Hg2) to form an Hg_6P_2 octahedron. The Hg_6P_2 octahedra share all corners to form a perovskite-like 3D octahedral network. The Cl2 atom, which we consider to belong to the cationic framework, is 2.854(4) Å from the nearest-neighbor atom Hg2 in the cationic framework and whose formula $(Hg_6P_4Cl_3)^+$ can be derived. The discrete triangular pyramidal guest $(PbCl_3)^-$ anions, which are comprised of the tricoordinated Pb1 by Cl1 atoms with a Pb−Cl bond length of 2.746(2) Å and have the shape of a pyramid with the Pb in a vertex, occupy half-cavities of the $_\infty^3(Hg_6P_4Cl_3)^+$ framework, with the neighboring ones remaining empty.

The 3D cationic network of **2** is built of two kinds of units. One is Hg_6P_2 triangular prisms, which have coordination geometry similar to that of Hg_6P_2 octahedra in **1** but with different cross-angles between two Hg_3 faces. The other one is (Hg_4P) tetrahedra, which are built of linearly coordinated Hg and tetrahedrally coordinated Pn atoms. The triangular prism and tetrahedral units with a ratio of 1:10 share all corners with each other to form 3D cationic framework $_\infty^3(Hg_{23}P_{12})^{12+}$ with 1D hexagonal tunnels along the c direction. The guest polyanion of **2** is built of a trigonal-bipyramidally coordinated split Zn to form a $(ZnCl_5)$ trigonal bipyramid, which is apex-shared with each other to form a 1D infinite $_\infty^1(ZnCl_4)^{2-}$ chiral chain, embedded in the tunnels of **2**.

The Hg−P and P−P bond lengths in the cationic moiety in **1** and **2** range from 2.304(9) to 2.451(3) Å and from 2.14(3) to 2.19(1) Å, which lie in the normal range for Hg−P and P−P bond lengths in known mercury pnictidohalides, respectively.[19]

dx.doi.org/10.1021/ic401056t | Inorg. Chem. 2013, 52, 8865−8871

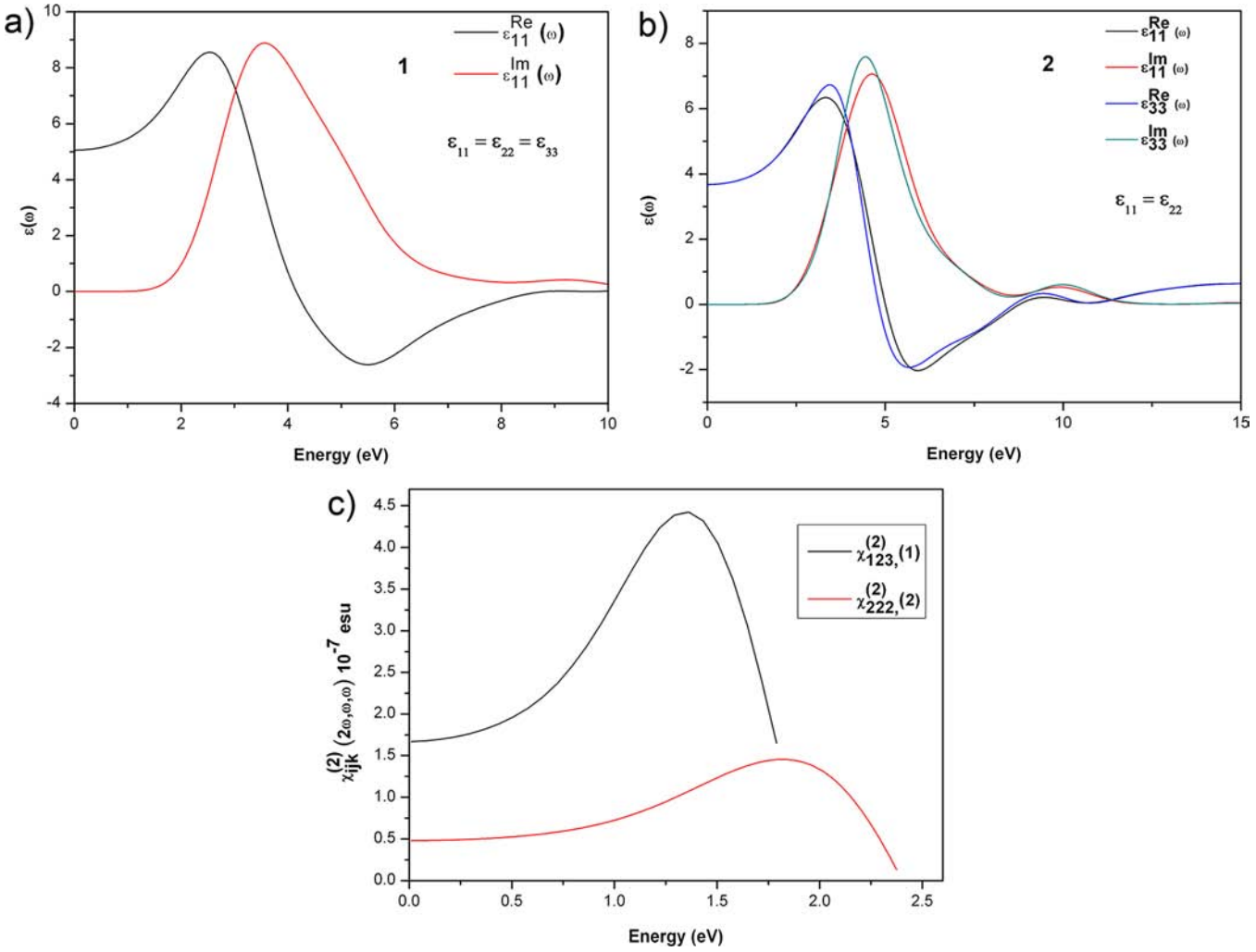

Figure 4. Calculated imaginary and real parts of dielectric functions of **1** (a) and **2** (b) in different polarization directions and calculated second-order susceptibilities (c) of **1** and **2**.

The Pb−Cl bond distance [2.745(5) Å], Hg−Cl bond distance [2.854(4) Å], and Zn−Cl bond distances [2.257(18)−2.377(13) Å] are close to those found in the literature.[19,20]

The distances between the cationic hosts and anionic guests in **1** and **2** are significantly longer than the expected values for covalent bonding, thus suggesting typical supramolecular interactions between them.[9] The shortest interatomic distances between the halogen atoms of the guest anions and the Hg atoms in the host frameworks of **1** and **2** are 2.894(4) and 2.941(3) Å, respectively, which are much longer than the Hg−Cl covalent bond length but shorter than the sum of the van der Waals radii of the Hg and Cl atoms. This indicates that there are weak supramolecular interactions between the cationic and anionic moieties in the crystal structures of **1** and **2**, as was the case found in the literature.[21] It can be seen from Table S2 in the SI that Zn1 and Zn2 atoms in **2** are equivalently split into two symmetric positions, which can be ascribed to the weak supramolecular interactions between the host and guest.

The noncentrosymmetric structures of **1** and **2** prompt us to measure their SHG properties. Powder SHG measurements on hand-selected crystalline samples were performed by using the Kurtz and Perry method with a 2.05 μm Q-switch laser.[22] The SHG signals as a function of the particle size from the measurements made on ground crystals of **1** and **2** are shown in Figure 2d. The result of **2** is consistent with type I phase-matching behavior according to the rule proposed by Kurtz and Perry, while compound **1** is non-phase-matching, which can be ascribed to the isotropy of the refractive index for its cubic crystal system. So, a quasi-phase-matching technique[23] is needed in the practical application of **1** for laser frequency conversion. A sample of $AgGaS_2$ (about 100 μm) was prepared as a reference material. The SHG efficiencies of **1** and **2** are about 2.5 and 1.1 times that of $AgGaS_2$ (d_{eff} = 12.5 pm V^{-1}),[24] respectively. It is well-known that the measured SHG signal intensity by the Kurtz and Perry powder method is proportional to the squares of the second-order nonlinear d_{eff} coefficient and that the second-order susceptibility $\chi^{(2)}_{eff}$ is twice that of the SHG coefficient d_{eff}, so the derived second-order susceptibilities $\chi^{(2)}_{eff}$ for **1** and **2** are 39.53 (9.49×10^{-8}) and 26.22 pm V^{-1} (6.29×10^{-8} esu), respectively, which corresponded to approximately 45 and 30 times as large as that of $\chi^{(2)}_{36}$ (KDP, 0.88 pm V^{-1}), respectively. The IR and optical diffuse-reflectance spectra show that compounds **1** and **2** are transparent in the IR range (0.8−25 μm; Figures 2b and S1 in the SI), which are comparable with those of well-known IR NLO crystals $AgGaS_2$ (0.48−11.4 μm) and $ZnGeP_2$ (0.74−12 μm). TGA curves indicate that compounds **1** and **2** are stable

dx.doi.org/10.1021/ic401056t | Inorg. Chem. 2013, 52, 8865−8871

up to about 230 and 280 °C (Figure S2 in the SI), respectively. Therefore, compound **2** may be a good candidate for mid- and far-IR NLO materials. Three different bond types, i.e., metal−pnicogen (Hg−P), metal−halogen (Hg−Cl), and pnicogen−pnicogen (P−P) for hosts and metal−halogen bonds (Pb−Cl and Zn−Cl) for guests, are assembled in the structures of **1** and **2** through supramolecular interactions, according to the above structure study. To the best of our knowledge, they are the first IR NLO compounds with simultaneously containing metal−pnicogen, pnicogen−pnicogen, and metal−halogen bonds in the structures.[3] This indicates that new IR NLO materials can be designed by combining two or more different bond types with no IR absorption within a single compound through supramolecular assembly and crystal engineering strategy.[25]

To gain further insight into the optical properties of **1** and **2**, theory studies including band structures and second-order NLO susceptibility calculations were performed by using the *CASTEP* code.[14]

The calculated band structures and DOSs of **1** and **2** along certain symmetry directions (Table S5 in the SI) are given in Figure 3. It can be seen from the band structure plot of **1** that the lowest energy (2.27 eV) of the conduction bands (CBs) is localized at the *X* point, while the highest energy (0.00 eV) of the valence bands (VBs) is localized at the *G* point. So, compound **1** is an indirect-band-gap material. Correspondingly, compound **2** is direct-band-gap because both the lowest energy (2.05 eV) of the CBs and the highest energy (0.00 eV) of the VBs are localized at the *G* point. The calculated band gaps of **1** and **2** using the local density approximation are E_g = 2.27 and 2.05 eV, which are smaller than the experimental values 2.30 and 2.29 eV (Figure 2c), respectively. So, scissors operators of 0.03 and 0.24 eV are obtained for calculations of the optical properties of **1** and **2**, respectively. The bands can be assigned according to the total and partial DOSs. For **1**, the band just above the Fermi level (or the bottom of the CB) is derived from unoccupied Hg 6s and P 3p states, mixing with a small amount of Pb 6p, Pb 6s, and Cl 3p states. The band just below the Fermi level is predominately composed of Cl 3p and P 3p states. For **2**, the band just above the Fermi level is predominately derived from unoccupied Hg 6s and P 3p states and the band just below the Fermi level is mainly composed of Cl 3p and P 3p states. Therefore, the optical absorptions are mainly ascribed to the charge transitions from Cl 3p and P 3p states to Hg 6s and P 3p states for both **1** and **2**.

The calculated imaginary part $\varepsilon_2(\omega)$ and the real part $\varepsilon_1(\omega)$ of the frequency-dependent optical dielectric functions of **1** and **2** are shown in parts a and b of Figure 4, respectively. Only one independent dielectric tensor is left for **1** because of its cubic system, namely, $\varepsilon_{11}(\omega) = \varepsilon_{22}(\omega) = \varepsilon_{33}(\omega)$, while **2** has two independent dielectric tensors, $\varepsilon_{11}(\omega)$ and $\varepsilon_{33}(\omega)$. It is found from dispersion of the calculated $\varepsilon_2(\omega)$ spectra that the onset energy of absorption is located at about 2.3 eV, for both **1** and **2**, corresponding to their experimental band gaps. The major absorption peaks located at about 3.6 and 4.5 eV on $\varepsilon_2(\omega)$ spectra of **1** and **2**, respectively, are contributed from the charge transfers from Cl 3p and P 3p states to Hg 6s and P 3p states according to DOS analysis. The space group of **1** belongs to class 23 and has only one nonvanishing independent second-order susceptibility tensors (χ_{123}) at low energy and under the restriction of Kleinman's symmetry. Correspondingly, the space group of **2** belongs to class $\bar{6}2m$ and also has only one nonvanishing independent second-order susceptibility tensor (χ_{222}). The calculated NLO susceptibilities χ_{123} for **1** and χ_{222} for **2** at a wavelength of 2.05 μm (0.59 eV) are 20.7×10^{-8} and 5.47×10^{-8} esu, respectively (Figure 4c), which are close to our experimentally derived χ_{eff} coefficients for **1** (9.49×10^{-8} esu) and **2** (6.29×10^{-8} esu) on the order, respectively.

4. CONCLUSIONS

In summary, two new different-bond-type hybrid compounds, $(Hg_6P_4Cl_3)(PbCl_3)$ and $(Hg_{23}P_{12})(ZnCl_4)_6$, with supramolecular interactions between host and guest moieties, which are based on metal−pnicogen (Hg−P), metal−halogen (Hg−Cl), and pnicogen−pnicogen (P−P) for hosts and metal−halogen bonds (Pb−Cl and Zn−Cl) for guests, were obtained by solid-state reactions. They exhibit band gaps of 2.30 and 2.29 eV, for **1** and **2**, respectively. Compounds **1** and **2** show large SHG activity of about 2.5 and 1.1 times that of $AgGaS_2$, respectively, at a laser wavelength of 2.05 μm and are transparent in the wide IR range (2.5−25 μm). Compound **2** shows type I phase-matching behavior, while **1** is non-phase-matching. It can be concluded that **2** may be a nominator for potential mid-IR NLO materials. Compounds **1** and **2** are the first IR NLO compounds with simultaneously containing metal−pnicogen, pnicogen−pnicogen, and metal−halogen bonds in the structures, providing an effective route for searching new IR NLO materials by combining two or more different bond types with no IR absorption within a single compound through supramolecular assembly and crystal engineering strategy.

■ ASSOCIATED CONTENT

Ⓢ Supporting Information

Details of crystallographic studies (CIF), atomic coordinates, select bond distance lengths, state energies, and UV diffuse-reflectance spectra. This material is available free of charge via the Internet at http://pubs.acs.org.

■ AUTHOR INFORMATION

Corresponding Author

*E-mail: gcguo@fjirsm.ac.cn.

Notes

The authors declare no competing financial interest.

■ ACKNOWLEDGMENTS

We gratefully acknowledge financial support by the NSF of China (Grants 90922035, 21003126, and 91222204), the Key Project from the CAS (Grant KJCX2-EW-H03), and the NSF of Fujian Province (Grant 2010H0022).

■ REFERENCES

(1) (a) Chen, C.; Liu, G. *Annu. Rev. Mater. Sci.* **1986**, *16*, 203. (b) Burland, D. M. *Chem. Rev.* **1994**, *94*, 1. (c) Pan, S.; Smit, J. P.; Watkins, B.; Marvel, M. R.; Stern, C. L.; Poeppelmeier, K. R. *J. Am. Chem. Soc.* **2006**, *128*, 11631. (d) Senechal-David, K.; Hemeryck, A.; Tancrez, N.; Toupet, L.; Williams, J. A. G.; Ledoux, I.; Zyss, J.; Boucekkine, A.; Guegan, J.-P.; Le Bozec, H.; Maury, O. *J. Am. Chem. Soc.* **2006**, *128*, 12243. (e) Babgi, B.; Rigamonti, L.; Cifuentes, M. P.; Corkery, T. C.; Randles, M. D.; Schwich, T.; Petrie, S.; Stranger, R.; Teshome, A.; Asselberghs, I.; Clays, K.; Samoc, M.; Humphrey, M. G. *J. Am. Chem. Soc.* **2009**, *131*, 10293.

(2) (a) Nikogosyan, D. N. *Nonlinear optical crystals: a complete survey*; Springer Science: New York, 2005. (b) Dmitriev, V. G.; Gurzadyan, G. G.; Nikogosyan, D. N. *Handbook of nonlinear optical crystals*, 3rd ed.; Springer: Berlin, 1999.

(3) Jiang, X.-M.; Guo, S.-P.; Zeng, H.-Y.; Zhang, M.-J.; Guo, G.-C. *Struct. Bonding (Berlin)* **2012**, *145*, 1.

(4) (a) Chen, C. W.; Hsu, Y. K.; Huang, J. Y.; Chang, C. S.; Zhang, J. Y.; Pan, C. L. *Opt. Express* **2006**, *14*, 10636. (b) Boyd, G. D.; Buehler, E.; Storz, F. G. *Appl. Phys. Lett.* **1971**, *18*, 301. (c) Boyd, G. D.; Kasper, H.; Mcfee, J. H. *IEEE J. Quantum Electron.* **1971**, *QE 7*, 563. (d) Lin, X.; Zhang, G.; Ye, N. *Cryst. Growth Des.* **2009**, *9*, 1186.

(5) (a) Kim, Y.; Seo, I. S.; Martin, S. W.; Baek, J.; Halasyamani, P. S.; Arumugam, N.; Steinfink, H. *Chem. Mater.* **2008**, *20*, 6048. (b) Liao, J. H.; Marking, G. M.; Hsu, K. F.; Matsushita, Y.; Ewbank, M. D.; Borwick, R.; Cunningham, P.; Rosker, M. J.; Kanatzidis, M. G. *J. Am. Chem. Soc.* **2003**, *125*, 9484. (c) Lekse, J. W.; Moreau, M. A.; McNerny, K. L.; Yeon, J.; Halasyamani, P. S.; Aitken, J. A. *Inorg. Chem.* **2009**, *48*, 7516. (d) Guo, S.-P.; Guo, G.-C.; Wang, M.-S.; Zou, J.-P.; Xu, G.; Wang, G.-J.; Long, X.-F.; Huang, J.-S. *Inorg. Chem.* **2009**, *48*, 7059. (e) Chen, M. C.; Wu, L. M.; Lin, H.; Zhou, L. J.; Chen, L. *J. Am. Chem. Soc.* **2012**, *134*, 6058. (f) Zhao, H. J.; Zhang, Y. F.; Chen, L. *J. Am. Chem. Soc.* **2012**, *134*, 1993. (g) Chen, M. C.; Li, L. H.; Chen, Y. B.; Chen, L. *J. Am. Chem. Soc.* **2011**, *133*, 4617.

(6) (a) Liu, T.; Qin, J.; Zhang, G.; Zhu, T.; Niu, F.; Wu, Y.; Chen, C. *Appl. Phys. Lett.* **2008**, *93*, 091102. (b) Tong, Y. Z.; Meng, X. Y.; Wang, Z. Z.; Chen, C. T.; Lee, J. M. H. *Appl. Phys.* **2005**, *98*, 033504. (c) Zhang, G.; Liu, T.; Zhu, T.; Qin, J.; Wu, Y.; Chen, C. *Opt. Mater.* **2008**, *31*, 110. (d) Ferrier, A.; Vela'zquez, M.; Doualan, J. L.; Moncorge, R. *Appl. Phys. B: Lasers Opt.* **2009**, *95*, 287. (e) Zhang, G.; Qin, J.; Liu, T.; Zhu, T.; Fu, P.; Wu, Y.; Chen, T. *Cryst. Growth Des.* **2008**, *8*, 2946. (f) Zhang, G.; Qin, J.; Liu, T.; Li, Y.; Wu, Y.; Chen, C. *Appl. Phys. Lett.* **2009**, *95*, 261104.

(7) (a) Chung, I.; Malliakas, C. D.; Jang, J. I.; Canlas, C. G.; Weliky, D. P.; Kanatzidis, M. G. *J. Am. Chem. Soc.* **2007**, *129*, 14996. (b) Bera, T. K.; Jang, J. I.; Ketterson, J. B.; Kanatzidis, M. G. *J. Am. Chem. Soc.* **2009**, *131*, 75. (c) Kim, Y.; Martin, S. W.; Ok, K. M.; Halasyamani, P. S. *Chem. Mater.* **2005**, *17*, 2046. (d) Guo, S.-P.; Guo, G.-C.; Wang, M.-S.; Zou, J.-P.; Zeng, H.-Y.; Cai, L.-Z.; Huang, J.-S. *Chem. Commun.* **2009**, 4366. (e) Zhang, Q.; Chung, I.; Jang, J. I.; Ketterson, J. B.; Kanatzidis, M. G. *J. Am. Chem. Soc.* **2009**, *131*, 9896. (f) Jiang, X.-M.; Zhang, M.-J.; Zeng, H.-Y.; Guo, G.-C.; Huang, J.-S. *J. Am. Chem. Soc.* **2011**, *133*, 3410. (g) Yu, P.; Zhou, L. J.; Chen, L. *J. Am. Chem. Soc.* **2012**, *134*, 2227.

(8) (a) Liu, G.; Zhao, Y. N.; Sun, C. H.; Li, F.; Lu, G. Q.; Cheng, H. M. *Angew. Chem., Int. Ed.* **2008**, *47*, 4516. (b) Ebenso, E. E. *Mater. Chem. Phys.* **2003**, *79*, 58.

(9) (a) Muller, A.; Reuter, H.; Dillinger, S. *Angew. Chem., Int. Ed. Engl.* **1995**, *34*, 2328. (b) Desiraju, G. R. *Angew. Chem., Int. Ed. Engl.* **1995**, *34*, 2311.

(10) (a) Ok, K. M.; Halasyamani, P. S. *Chem. Mater.* **2006**, *18*, 3176. (b) Halasyamani, P. S. *Chem. Mater.* **2004**, *16*, 3586. (c) Mao, J. G.; Jiang, H. L.; Kong, F. *Inorg. Chem.* **2008**, *47*, 8498.

(11) Rigaku. *CrystalClear*, version 1.3.5; Rigaku Corp.: Tokyo, 2002.

(12) Siemens. *SHELXLTL Reference Manual*, version 5; Siemens Energy & Automation Inc.: Madison, WI, 1994.

(13) (a) Wendlandt, W. W.; Hecht, H. G. *Reflectance Spectroscopy*; Interscience Publishers: New York, 1966. (b) Korüm. *Reflectance Spectroscopy*; Springer: New York, 1969.

(14) (a) Segall, M. D.; Lindan, P. L. D.; Probert, M. J.; Pickard, C. J.; Hasnip, P. J.; Clark, S. J.; Payne, M. C. *J. Phys.: Condens. Matter* **2002**, *14*, 2717. (b) Milman, V.; Winkler, B.; White, J. A.; Pickard, C. J.; Payne, M. C.; Akhmatskaya, E. V.; Nobes, R. H. *Int. J. Quantum Chem.* **2000**, *77*, 895.

(15) Perdew, J. P.; Burke, K.; Ernzerhof, M. *Phys. Rev. Lett.* **1996**, *77*, 3865.

(16) (a) Hamann, D. R.; Schluter, M.; Chiang, C. *Phys. Rev. Lett.* **1979**, *43*, 1494. (b) Lin, J. S.; Qteish, A.; Payne, M. C.; Heine, V. *Phys. Rev. B* **1993**, *47*, 4174.

(17) (a) Bassani, F.; Parravicini, G. P. *Electronic States and Optical Transitions in Solids*; Pergamon Press Ltd.: Oxford, U.K., 1975; pp 149−154. (b) Gajdos, M.; Hummer, K.; Kresse, G. *Phys. Rev. B* **2006**, *73*, 045112.

(18) Boyd, R. W. *Nonlinear Optics*; Academic Press: New York, 1992; pp 21−32.

(19) (a) Shevelkov, A. V.; Dikarev, E. V.; Popovkin, B. A. *J. Solid State Chem.* **1993**, *104*, 177. (b) Olenev, A. V.; Shevelkov, A. V. *J. Solid State Chem.* **2001**, *160*, 88. (c) Olenev, A. V.; Baranov, A. I.; Shevelkov, A. V.; Popovkin, B. A. *Eur. J. Inorg. Chem.* **2002**, *3*, 547.

(20) (a) Zou, J.-P.; Li, Y.; Fu, M.-L.; Guo, G.-C.; Xu, G.; Liu, X.-H.; Zhou, W.-W.; Huang, J.-S. *Eur. J. Inorg. Chem.* **2007**, *7*, 977. (b) Léger, J. M.; Haines, J.; Atouf, A. *Phys. Rev. B* **1995**, *51*, 3902. (c) Olenev, A. V.; Shevelkov, A. V.; Popovkin, B. A. *Zh. Neorg. Khim.* **1999**, *44*, 1853.

(21) (a) Olenev, A. V.; Shevelkov, A. V. *Angew. Chem., Int. Ed.* **2001**, *40*, 2353. (b) Zou, J.-P.; Wu, D.-S.; Huang, S.-P.; Zhu, J.; Guo, G.-C.; Huang, J.-S. *J. Solid State Chem.* **2007**, *180*, 805. (c) Zou, J.-P.; Li, Y.; Zhang, Z.-J.; Guo, G.-C.; Liu, X.; Wang, M.-S.; Cai, L.-Z.; Lu, Y.-B.; Huang, J.-S. *Inorg. Chem.* **2007**, *46*, 7321.

(22) Kurtz, S. K.; Perry, T. T. *Appl. Phys.* **1968**, *39*, 3798.

(23) (a) Koh, S.; Kondo, T.; Shiraki, Y.; Ito, R. *J. Cryst. Growth* **2001**, *227*, 183. (b) Bliss, D. F.; Lynch, C.; Weyburne, D.; O'Hearn, K.; Bailey, J. S. *J. Cryst. Growth* **2006**, *287*, 673. (c) Yu, X. J.; Scaccabarozzi, L.; Lin, A. C.; Fejer, M. M.; Harris, J. S. *J. Cryst. Growth* **2007**, *301*, 163.

(24) Zondy, J.-J.; Touahri, D.; Acef, O. *J. Opt. Soc. Am.* **1997**, *B14*, 2481.

(25) (a) Rogers, R. D.; Bond, A. H.; Aguinaga, S.; Reyes, A. *J. Am. Chem. Soc.* **1992**, *114*, 2967. (b) Cariati, E.; Ugo, R.; Cariati, F.; Roberto, D.; Masciocchi, N.; Galli, S.; Sironi, A. *Adv. Mater.* **2001**, *13*, 1665. (c) Xu, G.; Li, Y.; Zhou, W.-W.; Wang, G.-J.; Long, X.-F.; Cai, L.-Z.; Wang, M.-S.; Guo, G.-C.; Huang, J.-S.; Bator, G.; Jakubas, R. *J. Mater. Chem.* **2009**, *19*, 2179.